QUANTITATIVE ASSESSMENT OF THE RISK OF AIRBORNE TRANSMISSION OF SARS-CoV-2 INFECTION: PROSPECTIVE AND RETROSPECTIVE APPLICATIONS

G. Buonanno[1,2], L. Morawska[2], L. Stabile[1,*]

[1] Department of Civil and Mechanical Engineering, University of Cassino and Southern Lazio, Cassino, FR, Italy

[2] International Laboratory for Air Quality and Health, Queensland University of Technology, Brisbane, Qld, Australia

***Corresponding author:**

Luca Stabile

Department of Civil and Mechanical Engineering,

University of Cassino and Southern Lazio, Cassino, FR, Italy

Via G. Di Biasio 43, 03043 Cassino (FR), Italy

e-mail: l.stabile@unicas.it

Abstract

Airborne transmission is a recognized pathway of contagion; however, it is rarely quantitatively evaluated. This study presents a novel approach for quantitative assessment of the individual infection risk of susceptible subjects exposed in indoor microenvironments in the presence of an asymptomatic infected SARS-CoV-2 subject. The approach allowed the maximum risk for an exposed healthy subject to be evaluated or, starting from an acceptable risk, the maximum

exposure time. We applied the proposed approach to four distinct scenarios for a prospective assessment, highlighting that, in order to guarantee an acceptable individual risk of 10^{-3} for exposed subjects in naturally ventilated indoor environments, the exposure time should be shorter than 20 min. The proposed approach was used for retrospective assessment of documented outbreaks in a restaurant in Guangzhou (China) and at a choir rehearsal in Mount Vernon (USA), showing that, in both cases, the high attack rate values can be justified only assuming the airborne transmission as the main route of contagion. Moreover, we shown that such outbreaks are not caused by the rare presence of a superspreader, but can be likely explained by the co-existence of conditions, including emission and exposure parameters, leading to a highly probable event, which can be defined as a "superspreading event".

Keywords: SARS-CoV-2 (COVID-19) assessment; virus airborne transmission; indoor; ventilation; coronavirus.

1. Introduction

The airborne transmission of a virus and the consequent contagion risk assessment is a complex issue that requires multidisciplinary knowledge. It is necessary to understand the characteristics and mechanisms behind the generation of respiratory microdroplets [1,2], the survival of viruses in microdroplets [3], the transport of microdroplets and human exposure to them [4], and the airflow patterns that carry microdroplets in buildings [5]. Expiratory human activities generate virus-carrying microdroplets that are small enough to remain aloft in air during exhalation, talking, and coughing [2,6,7]. Atomization occurs in the respiratory tract, and droplets are expelled at high speed during expiration [8,9]. Toques of liquid originating from different areas of the upper respiratory tract are drawn out from the surface and broken into droplets of different sizes [10]. The findings of

48 early investigations [11–13] served as a foundation for subsequent studies involving temporal and
49 spatial visualization methods using high-speed cameras [14], particle image velocimetry [8] and, above
50 all, increasingly accurate particle counters [6], which have facilitated the detailed characterization
51 and quantitation of droplets expelled during various forms of human respiratory exhalation flows.
52 The issue of the viral load emitted, however, remained difficult to solve. In the past, backward
53 calculation was used to estimate the emission of an infected subject based on retrospective
54 assessments of infectious outbreaks only at the end of an epidemic [15–18]. This led to the definition
55 of emission values for each virus regardless of the type of respiratory act and the metabolic
56 activity of the infected subject. Recently, the authors presented an approach to evaluate the viral
57 load emitted by infected individuals with a view to provide new predictive capacities, not currently
58 available [19]. This approach, based on the oral viral load and the infectivity of the virus, takes into
59 account the effect of other parameters such as inhalation rate, type of respiratory activity, and
60 activity level, to estimate the quanta emission rate. This value provides key information for
61 engineers and indoor air quality experts to simulate airborne dispersion of diseases in indoor
62 environments. Indeed, the use of exposure risk models in closed environments [20,21] makes it
63 possible to estimate contagion starting from the emission values of a contagious subject.
64 The overall approach of emission and exposure modelling represents an essential tool to be
65 applied in enclosed spaces, and can support air quality experts and epidemiologists in the
66 management of indoor environments during an epidemic for both prospective and retrospective
67 assessments.
68 In this paper we apply a novel approach that takes into account the characteristics of the emitting
69 subject, the microenvironment, and the exposed subject to calculate the probability of infection
70 and the individual risk, for both prospective and retrospective assessments of airborne infectious
71 transmission of SARS-CoV-2. In the case of prospective assessment, various exposure scenarios in

indoor environments were analyzed in order to assess the influence of risk mitigation parameters. In the case of retrospective assessment, we estimated the probability of infection and the individual risk of two documented outbreaks.

2. Materials and methods

To evaluate both prospective and retrospective assessments of the airborne transmission of SARS-CoV-2, we used a four-step approach to quantify the probability of infection, i.e. the ratio between infected cases and the exposed population due to exposure in a microenvironment where a SARS-CoV-2 infected subject is present. The four steps of the proposed approach are: i) evaluation of the quanta emission rate; ii) evaluation of the exposure to quanta concentration in the microenvironment; iii) evaluation of the dose of quanta received by an exposed susceptible subject; and iv) estimation of the probability of infection on the basis of a dose–response model. The simulations of the probability of airborne transmission of SARS-CoV-2 were performed applying a Monte Carlo method [22]. Further they adopted the infection risk assessment typically implemented to evaluate the transmission dynamics of infectious diseases and to predict the risk of these diseases to the public [17,20,21].

Once the probability of infection was obtained, an approach to evaluate the individual infection risk, i.e. a parameter that also takes into account how likely the probability of infection can occur, was also implemented. Individual risk can be easily compared to an acceptable risk, i.e. a target reference risk that could be suggested by agencies and regulatory authorities to control the pandemic. In the following sections, the methodologies adopted to evaluate the probability of infection based on the four step approach (section 2.1) and the individual infection risk (section 2.2) are described. The application of the proposed approach for prospective and retrospective assessments is described in sections 2.3 and 2.4.

2.1 Estimation of the probability of infection

2.1.1 Evaluation of the quanta emission rate: the forward emission approach

Recently, Buonanno et al. [19] proposed a forward emission approach to estimate the quanta emission rate of an infectious subject on the basis of the viral load in the sputum and the concentration of droplets expired during different activities. A quantum is defined as the dose of airborne droplet nuclei required to infect a susceptible person. The quanta emission rate (ER_q, quanta h^{-1}) was evaluated as:

$$ER_q = c_v \cdot c_i \cdot IR \cdot \int_0^{10\mu m} N_d(D) \cdot dV_d(D) \quad (1)$$

where c_v is the viral load in the sputum (RNA copies mL^{-1}), c_i is a conversion factor defined as the ratio between one infectious quantum and the infectious dose expressed in viral RNA copies, *IR* is the inhalation rate ($m^3\ h^{-1}$), N_d is the droplet number concentration (part. cm^{-3}), and $V_d(D)$ is the volume of a single droplet (mL) as a function of the droplet diameter (D). The number and volume of the droplets (V_d) is determined on the basis of data obtained experimentally by Morawska et al. (2009)[6].

With reference to the SARS-CoV-2 viral load in the mouth, researchers have recently found c_v values of up to 10^{11} copies mL^{-1}, which is also variable in the same patient during the course of the disease [23–26]. In particular, Rothe et al. [24] reported a case of SARS-CoV-2 infection in which transmission appears to have occurred during the incubation period in the index patient. A high viral load of 10^8 copies mL^{-1} was found, confirming that asymptomatic persons are potential sources of SARS-CoV-2 infection. Furthermore, Pan et al. [23], in a study on 82 SARS-CoV-2 infected patients, found c_v values in the range of 10^8–10^9 RNA copies mL^{-1}, also in the previous days and in the first days of onset of the disease. Consequently, the concentrations of the viral load in the

mouth can reach values of 10^9 RNA copies $mL^{-1}$and occasionally up to 10^{11} RNA copies mL^{-1} during the course of the disease.

The conversion factor, c_i, i.e. the ratio between one infectious quantum and the infectious dose expressed in viral RNA copies, barely represents the probability of a pathogen surviving inside the host to initiate the infection; thus c_i=1 implicitly assumes that infection will occur for each pathogen (RNA copy in the case of SARS-CoV-2) received by the exposed people. There are currently no values available in the scientific literature for c_i for SARS-CoV-2. Watanabe et al. [27] estimated the infectious doses of several coronaviruses on the basis of data sets challenging humans with virus HCoV-229E (known as an agent of human common cold) and animals with other viruses (e.g. mice with MHV-1, considered as a surrogate of SARS-CoV-1). On the basis of the orders of magnitude of the infectivity conversion factors for the overall data sets, we assumed a c_i range between 0.01 and 0.1.

The quanta emission rate calculation was performed for four different emission profiles (which are adopted in the risk evaluations described later) evaluated as a combination of expiratory activities and activity levels: (i) oral breathing during resting; (ii) oral breathing during heavy activity; (ii) speaking during light activity; and (iv) singing (or loudly speaking) during light activity.

Quanta emission rates were calculated using eq. (1) and applying a Monte Carlo method [22] in order to take into account for the possible variation of the input data. To this end, probability density functions characteristics of each parameter were considered. In particular, we considered normal distributions for: (i) the log-transformed c_v data (average and standard deviation of $\log_{10}(c_v)$ equal to 8 and 0.7 $\log_{10}$ (RNA copies mL^{-1}), respectively); and (ii) the infectious dose c_i (average and standard deviation equal to 0.025 and 0.125, respectively). A distribution of quanta emission rates (ER_q), was obtained as a result of application of the Monte Carlo method (Figure 1), i.e. the probability density function of ER_q (pdf_q).

142 *2.1.2 Evaluation of the exposure to quanta concentration*

143 The second step in evaluating the probability of infection is evaluation of the quanta
144 concentration to which a susceptible subject is exposed. The quanta concentration at time *t*, *n*(*t*),
145 in an indoor environment is based on the quanta mass balance proposed by Gammaitoni and
146 Nucci [20], and can be evaluated as:

147

148 $$n(t) = \frac{ER_q \cdot I}{IVRR \cdot V} + \left(n_0 - \frac{ER_q \cdot I}{IVRR}\right) \cdot \frac{e^{-IVRR \cdot t}}{V} \quad \text{(quanta m}^{-3}\text{)} \quad (2)$$

149 where *IVRR* (h^{-1}) represents the infectious virus removal rate in the space investigated, n_0
150 represents the initial number of quanta in the space, *I* is the number of infectious subjects, *V* is the
151 volume of the indoor environment considered, and ER_q is the quanta emission rate (quanta h^{-1}) for
152 the specific disease/virus under investigation. The quanta concentration calculation adopted here
153 is based on the following hypotheses: the quanta emission rate is considered to be constant, the
154 latent period of the disease is longer than the time scale of the model, and the droplets are
155 instantaneously and evenly distributed in the room [20]. The infectious virus removal rate is the sum
156 of three contributions [28]: the air exchange rate (AER) via ventilation, the particle deposition on
157 surfaces (*k*, e.g. via gravitational settling), and the viral inactivation (λ). The deposition rate was
158 evaluated as the ratio between the settling velocity of super-micrometric particles [roughly
159 1.0×10^{-4} m s^{-1} as measured by Chatoutsidou and Lazaridis [29]] and the height of the emission
160 source (1.5 m); thus, *k* was 0.24 h^{-1}. The viral inactivation was evaluated on the basis of the SARS-
161 CoV-2 half-life (1.1 h) detected by van Doremalen et al.[3], thus λ was 0.63 h^{-1}.
162 In the exposure scenarios tested with the prospective and retrospective approaches, to take the
163 variability of the input parameters into account, the indoor quanta concentration *n*(t) was
164 determined through eq. (2), applying a Monte Carlo method that adopted the probability density
165 functions (pdf_q) characteristic of quanta emission rates (ER_q). Since the probability density

functions of the log-transformed $\log_{10}(ER_q)$ for the different expiratory activities resulted in a normal distribution (Shapiro-Wilk test, $p < 0.01$), the quanta concentration $n(t)$ was evaluated by providing a Gaussian distribution of $\log_{10}(ER_q)$ (average and standard deviation values are is summarized in the results section; see Table 2) and then applying a back-transformation from $\log_{10}(ER_q)$ to ER_q. The relative frequency at which a certain quanta concentration occurred for each time step of simulation, i.e. the probability density function of the quanta concentration (pdf_n), was also obtained as result of the Monte Carlo simulations.

2.1.3 Evaluation of the dose of quanta received by an exposed susceptible subject

The dose of quanta received by a susceptible subject exposed to a certain quanta concentration, $n(t)$, for a certain time interval, T, can be evaluated by integrating the quanta concentration over time as:

$$D_q = IR \int_0^T n(t)dt \qquad \text{(quanta)} \qquad (3)$$

It can be concluded from Eq. (3) that the dose of quanta received by a susceptible subject is affected by the inhalation rate (IR) and subsequently by their activity level. As an example, for the same exposure scenario [i.e. identical $n(t)$ and T], the dose of quanta received by subjects performing at a light activity level ($IR = 1.38\ m^3\ h^{-1}$; e.g. slowly walking) is more than double that received by people just sitting or standing ($IR = 0.54\ m^3\ h^{-1}$). For the dose, in the exposure scenarios described in this paper, the Monte Carlo method was applied to eq. (3) considering the probability density function of the quanta concentration (pdf_n), whereas the IR was considered as a constant value; thus, the probability density function of the dose (pdf_D) was obtained for each time step of the simulation.

2.1.4 *Evaluation of the probability of infection through a dose–response model*

The fourth and final step in evaluating the probability of infection is the adoption of a dose–response model. Several dose–response models are available in the scientific literature for assessing the probability of infection of airborne-transmissible pathogens [16,17], including deterministic and stochastic models, and threshold and non-threshold models.

The best-suited dose–response models for airborne transmission of pathogens are the stochastic models. In particular, exponential models have been mostly adopted in previous studies because of their suitability and simplicity [27]. Such models consider the pathogens as discrete bundles (i.e. quanta) distributed in a medium (e.g. saliva/sputum) in a random manner described by the Poisson probability distribution. When the medium is aerosolized, the pathogen distribution in the aerosols, and hence their distribution in the air, also follows the Poisson probability distribution. The complex Poisson summation equations can be simplified in an exponential equation [17,27,30], i.e. the exponential dose–response model, which evaluates the probability of infection, P_I (%), of susceptible people as:

$$P_I = 1 - e^{-D_q} = \frac{C}{S} \quad (\%) \tag{4}$$

For a unit dose of quanta ($D_q = 1$), the probability of infection P_I is equal to 63%, from which derives the definition of "quantum" as the "amount of infectious material to infect $1\text{-}e^{-1}$ (i.e. 63%) of the people in an enclosed space" [13,20].

In the exponential dose–response model, the variation of host sensitivity to the pathogen is not considered. More complex models, such as the Beta-Poisson probability distribution, could take this factor into account [17,27,30]; nonetheless, in the present paper the differences in the exposed population in terms of susceptibility to the virus will not be considered.

The probability of infection P_I evaluated in the following exposure scenarios was determined through eq. (4), also applying a Monte Carlo method. To this end, the probability density functions of the dose of quanta (pdf_D) obtained as a result of the Monte Carlo simulation on D_q were considered; thus, a probability density function of P_I was also obtained (pdf_P).

The probability of infection represents the ratio between the number of infection cases (C) and the number of exposed susceptibles (S). In retrospective analyses of documented outbreaks, the known C/S ratio is typically defined as the "attack rate".

2.2 The individual infection risk and the basic reproduction number

As stated above, the probability of infection (P_I) is the expected number of infection cases in relation to the number of exposed susceptibles (C/S ratio). However, based on eqs. (2-4), such probability is strongly influenced by the probability density function of the dose (pdf_D), which is influenced in turn by the probability density function of the quanta concentration (pdf_n) and by the probability density function of the quanta emission rate (pdf_q). In other words, for a given exposure scenario (microenvironment, ventilation, inhalation rate of the exposed subject, etc.) the probability of infection (P_I) can assume different values on the basis of the rate of quanta emitted by the infected subject: the lower the quanta emission rates, the lower the probability of infection (since all the other parameters affecting the exposure were considered to be constant values). Thus, when evaluating the individual risk (R) of an exposed person, we should know both the probability of infection (P_I) and the probability of occurrence of such a P_I value (P_P). The latter is defined by the probability density function pdf_P. Since the probability of infection (P_I) and the probability of occurrence P_P are independent events, the individual infection risk, R, can be evaluated as the product of the two terms:

$$R = P_I \cdot P_P \quad (\%) \tag{5}$$

The probability density function of the individual risk, pdf_R, can be obtained by multiplying all the possible P_I values obtained from the application of the Monte Carlo method to the four-step approach by the corresponding probability of occurrence. The maximum value of R in eq. (5), i.e. the mode of the pdf_R, is of particular interest because it represents the most probable individual risk for a healthy subject or, in other words, the highest probability of being infected. In a conservative application of the proposed approach to estimate and reduce the risk of individuals being together with an infected individual in an indoor environment, the maximum individual infection risk must be less than an acceptable risk.

The US Environmental Protection Agency (EPA) typically uses a target reference risk range of 10^{-4} to 10^{-6} for carcinogens in drinking water [31], which is in line with World Health Organization (WHO) guidelines for drinking water quality, which base guideline values for genotoxic carcinogens on the upper bound estimate of an excess lifetime cancer risk of 10^{-5} [32]. If the estimated lifetime cancer risk is lower than 10^{-6}, the risk is considered acceptable, while risks above 10^{-4} are considered unacceptable [33].

The choice of an acceptable contagion risk for SARS-CoV-2 is difficult and certainly questionable. However, considering the mortality rate of SARS-CoV-2, this turns out to be an order of magnitude lower than the corresponding value associated with carcinogenic diseases. For this reason, only for discussion purposes, the value of 10^{-3} is taken as an acceptable risk reference for SARS-CoV-2.

For the purpose of managing an epidemic and keeping the infection under control, it is also important to estimate the basic reproduction number of the infection, R_0, which is calculated as the ratio between the number of susceptible people infected (C) and the infected subject (I). Thus, R_0 can be easily evaluated by multiplying the infection probability, P_I, by the number of exposed susceptible individuals (S). To control an epidemic, the R_0 value must be less than 1. Therefore, in

addition to estimating an acceptable individual infection risk, it is necessary to specifically verify that, with the crowding expected within the environment, the corresponding value of R_0 is less than 1.

2.3 Scenarios in the prospective assessment

The proposed four-step approach was applied to different indoor microenvironments by varying the main parameters in order to evaluate the effect of the influencing parameters. In particular, four emission profiles of the infected subject [6] and corresponding profiles of the healthy subjects exposed were chosen. For the sake of simplicity, the simulations were run assuming that the susceptible subjects remained in the microenvironment for the same length of time as the infected subject (i.e. the two subjects enter and leave the environment under test together). Each indoor environment under investigation was tested for three different values of air exchange rate (AER). Table 1 presents a detailed summary of the four different indoor exposure scenarios considered to evaluate the risk of airborne transmission of SARS-CoV-2. Scenario A consists of a hospital room of 100 m^3 where a resting infected patient emits quanta in the room through oral breathing, whereas the exposed susceptible subjects consist of a member of the medical staff in a light exercise activity (scenario A-1) and another patient at rest (scenario A-2). In scenario B, the infection affects two subjects, both oral breathing during a sports activity in a 300 m^3 gym. Scenario C concerns two subjects (infected and healthy) in light activity while speaking in a generic 300 m^3 office (bank, post office, supermarket, shop, etc.). Finally, scenario D represents an infected subject singing or speaking loudly in an 800 m^3 room with healthy subjects listening at a sedentary activity level.

Table 1 - Description of the exposure scenarios tested in the prospective assessment.

	Scenario A	Scenario B	Scenario C	Scenario D

Type of indoor environment	Hospital room	Gym	Public indoor environments (e.g. restaurant, bank)	Conference room or auditorium
Emitting subject	Patient (Resting, oral breathing)	Exercising person (heavy exercise, oral breathing)	Speaking person (light exercise, voiced counting)	Singer or conference loud speaker (light exercise, unmodulated vocalization)
Exposed subject	A-1. Medical staff (light exercise) A-2. Patient (resting)	Exercising person (heavy exercise)	Speaking person (light exercise)	Spectator (sedentary activity)
Volume (m^3)	100	300	300	800
Ventilation, AER (h^{-1})	• Natural ventilation 0.5 h^{-1}, • Mechanical ventilation 3 h^{-1}, • Mechanical ventilation 10 h^{-1}			
Deposition rate, k (h^{-1})	0.24			
Inactivation rate, λ (h^{-1})	0.63			

2.4 Retrospective assessments: outbreaks in a restaurant in Guangzhou, China, and at choir rehearsal in Skagit Valley (USA)

2.4.1 The outbreak in a restaurant in Guangzhou, China

A possible case of airborne transmission was recently documented by Lu et al.[34]. Here, an index case patient traveled from the Chinese epidemic epicenter, Wuhan, on 23 January 2020 and ate lunch in a restaurant in Guangzhou, China, with his family on 24 January 2020 (family A, 10 people sitting at the same table). Later that day, the index patient experienced onset of fever and cough and SARS-CoV-2 infection was diagnosed. On the following days, nine other people were diagnosed with SARS-CoV-2 infection: four members from family A's table and five other people at

two different tables (families B and C). No other customers seated at other tables or waiters were infected.

The restaurant is a 5-floor building without windows; each floor has its own air ventilation system. The third floor dining area, at which the index patient ate lunch, has a floor area of 145 m^2, with 15 tables arranged with a distance between each table of about 1 m. A total of 91 people (83 customers, 8 staff members) were in the room during that lunch. The exposure time was variable for the customers: those seated at tables close to the index patient had exposure times of 53 minutes (family B) and 73 minutes (family C). The ventilation and air conditioning situation is reported in Lu et al.[34]. Five fan coil air-conditioning units are installed in the room and there is no outdoor air supply; thus, the ventilation relies only upon infiltration and natural ventilation. The authors performed computational fluid dynamics analyses and tracer gas decay tests to obtain more information about the possible air-flow pathway in the room, and to determine the air exchange rate expected during that lunch. The analyses performed showed that, due to the particular installation and use of the fan coils, the room can be divided into different air-flow zones, with well-mixed conditions. The air-flow zone involving the table at which the index patient sat also included the two tables at which the other five infected people sat; and covered an area of roughly 45 m^3. The tracer gas decay tests revealed a low air exchange rate (mostly due to the absence of an outdoor air supply) in the range of 0.56–0.77 h^{-1}.

Therefore, on the basis of the available information, the retrospective assessment was applied to this outbreak case, through eqs. (2) and (3), using the following input data: i) room volume of 45 m^3; ii) documented probability of infection, i.e. attack rate, of 45% (i.e. 5 out of 11 people of families B and C (family A members were excluded as they could easily have been infected through other infection routes); iii) average exposure time of 1 h; iv) speaking at a light activity level for all people (both emitting and exposed subjects), and v) average AER = 0.67 h^{-1}.

2.4.2 The outbreak at a choir rehearsal in Skagit (USA)

A further possible case of airborne transmission of SARS-CoV-2 was documented by the USA media (www.latimes.com/world-nation/story/2020-03-29/coronavirus-choir-outbreak). This case was recorded on 10 March, in Mount Vernon (Skagit County, Washington State, USA). In a 810 m^3 hall, 61 choir members (out of a total of 121 regular members) gathered to rehearse, aware of the practices for the containment of contagion (frequent hand washing and social distancing). None of the members that attended had evident symptoms of SARS-CoV-2 infection. There was hand sanitizer at the front door and members refrained from the usual hugs and handshakes; each person brought their own sheet music. The event lasted from 6:30 pm to 9:00 pm (about 2.5 hours). Within few days, 33 of the 61 participants (53%) were diagnosed with SARS-CoV-2 infection, at least three were hospitalized, and two died [35].

As pointed out by Hamner et al.[35], the 2.5-hour singing practice could have provided several opportunities for droplet and fomite transmission (e.g. members sitting close to one another, sharing snacks, and stacking chairs at the end of the practice). Nonetheless, the abovementioned voluntary measures put in place would not support the documented spread of the contagion. On the contrary, the act of singing, itself, might have contributed to transmission through emission of aerosols, which is affected by loudness of vocalization [19]. This is even more relevant considering that attack rate of 53.3% (based on 33 confirmed cases) could represent a conservative estimate, since other 20 probable cases were mentioned by Hamner et al.[35].

As regard the heating and ventilating system, limited information is available: the Fellowship Hall is heated by a relatively new commercial forced-air furnace with supply and return air grills situated high on a single wall. The furnace is installed to have both make-up and combustion air, but it is not known how much fresh air was provided on that evening. During the entire rehearsal no exterior doors were open. We applied a retrospective assessment to the case of the Skagit

Valley choir through eqs. (2) and (3), using the following input data: i) room volume of 810 m^3; ii) documented probability of infection, i.e. attack rate, equal to 53%; iii) exposure time of 2.5 h; iv) singing at a light activity level for all people; and v) natural ventilation with an AER = 0.5 h^{-1}.

3. Results and Discussions

3.1 Statistics of quanta emission rates

Figure 1 and Table 2 show the statistics relating to the quanta emission rates for the four emission profiles considered in section 2.1. As shown in Buonanno et al.[19], there are large differences between the emission profiles. Obviously the lowest values are found under the oral breathing condition during resting (median value of 0.36 quanta h^{-1}), followed by the oral breathing condition during heavy activity as the inhalation rate increases (2.4 quanta h^{-1}), and reaching 4.9 quanta h^{-1} for the increase in aerosol emitted during vocalization [6] and, finally, peaking during singing/speaking loudly (31 quanta h^{-1}). Indeed, the rate of particle emission during normal human speech is positively correlated with the amplitude of vocalization [36].

The probability density functions of the quanta emission rates (P_q) were also determined. In particular, the log-transformed ER_q values obtained from the Monte Carlo simulations resulted in a normal distribution (Shapiro-Wilk test, $p < 0.01$). Table 2 shows the average and standard deviation values of the $\log_{10}(ER_q)$.

We point out that the estimated values present two main uncertainty contributions clearly related to the limited data currently available for the SARS-CoV-2: i) a still low number of experimental data for the viral load in the mouth, c_v, of SARS-CoV-2 infected subjects, ii) unavailable infectivity conversion factors, c_i, for SARS-CoV-2; indeed, as mentioned in the methodology section, the c_i parameter was estimated on the basis of data available for other coronaviruses challenging humans (only in the case of HCoV-229E) and animals (for all other types of coronavirus).

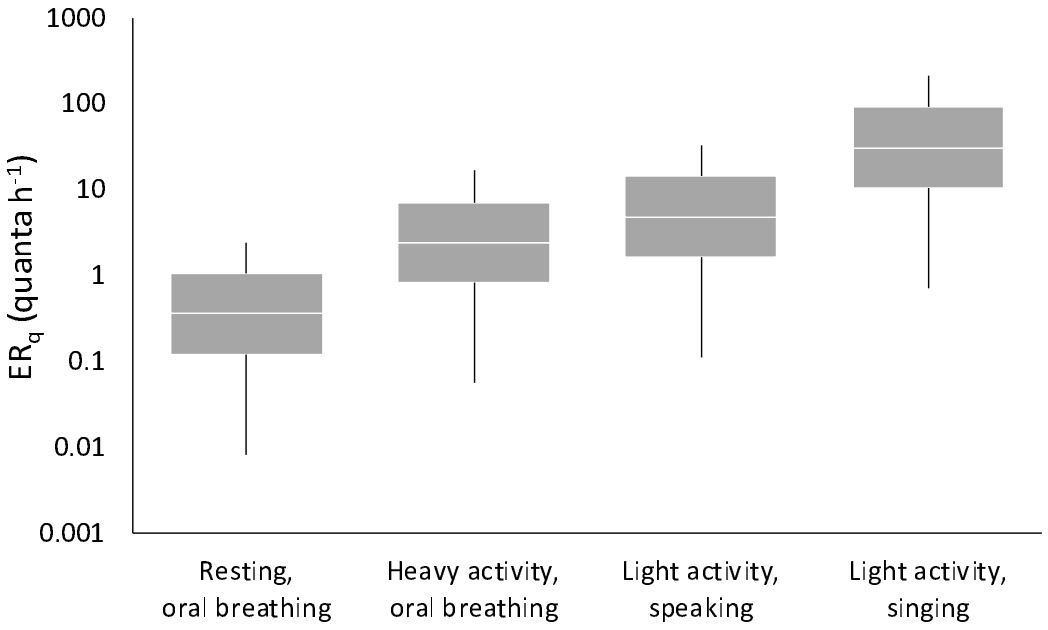

Figure 1 - Statistics of quanta emission rates (ER_q) for the four expiratory activities considered in the exposure scenarios. Data reported represent 1st, 25th, 50th, 75th, and 99th percentiles.

Table 2 - ER_q (quanta h^{-1}) and $\log(ER_q)$ statistics for SARS-CoV-2 as a function of the expiratory activity and activity level. The log-transformed ER_q values follow a log-normal distribution; thus, the average and standard deviation values of the $\log_{10}(ER_q)$ are provided.

		Resting, oral breathing	Heavy activity, oral breathing	Light activity, speaking	Light activity, singing (or speaking loudly)
ER_q	5th percentile	2.5×10^{-2}	1.7×10^{-1}	3.4×10^{-1}	2.1×10^{0}
	25th percentile	1.2×10^{-1}	8.1×10^{-1}	1.6×10^{0}	1.0×10^{1}
	50th percentile	3.6×10^{-1}	2.4×10^{0}	4.9×10^{0}	3.1×10^{1}
	75th percentile	1.1×10^{0}	7.2×10^{0}	1.5×10^{1}	9.3×10^{1}
	95th percentile	5.2×10^{0}	3.0×10^{1}	7.1×10^{1}	4.5×10^{2}
	99th percentile	1.6×10^{1}	1.1×10^{2}	2.2×10^{2}	1.4×10^{3}
$\log_{10}(ER_q)$	Average	-4.4×10^{-1}	3.9×10^{-1}	6.9×10^{-1}	1.5×10^{0}
	Stand. dev	7.1×10^{-1}	7.1×10^{-1}	7.1×10^{-1}	7.1×10^{-1}

3.2 *Risk management in prospective assessment applications*

3.2.1 *Illustrative example of probability of infection and individual risk evaluation*

In Figure 2 an illustrative example of quanta concentration $n(t)$, dose of quanta (D_q), and probability of infection (P_I) trends as a function of time (here shown for 2 h) resulting from the Monte Carlo simulation for exposure scenario D (singing exhibition, conference speaker) with an AER = 0.5 h^{-1} is shown. In particular, the trends of different percentiles are reported. The example shows that a person singing/speaking loudly in such a microenvironment can lead to a median $n(t)$ value after 2 hours equal to 0.027 quanta h^{-1} (with a 5^{th}–95^{th} percentile range of < 0.002–0.38 quanta h^{-1}). Such concentrations lead to a median dose of quanta received by the subject exposed for 2 h in a sedentary activity equal to 0.029 quanta (with a 5^{th}–95^{th} percentile range of < 0.002–0.42 quanta), then resulting in a median probability of infection, P_I, of 2.8% (with a 5^{th}–95^{th} percentile range of 0.2%–33.0%). Thus, if higher quanta emission rates are considered, the indoor quanta concentrations and the consequent probability of infection can be more than 10-fold the median values.

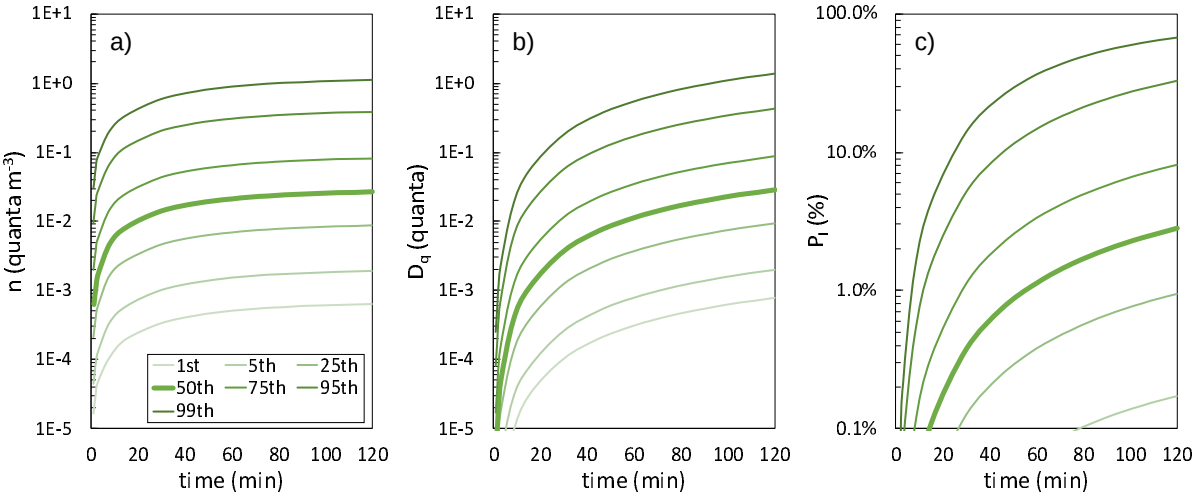

Figure 2 - Trends of quanta concentration (a), dose of quanta (b), and probability of infection (c) as a function of time (here shown for 2 h of exposure) resulting from the Monte Carlo simulation for exposure scenario D with an AER = 0.5 h^{-1}. Different percentiles are reported.

In view of the application of a conservative approach that could be essential to reduce the risk of contagion in indoor environments, using the highest quanta concentration and probability of infection values can be misguiding. Indeed, the probability of occurrence of such high values is extremely low. Thus, as described in section 2.2, a proper evaluation of the individual infection risk (R) can be obtained by applying eq. (4), i.e. multiplying the probability of infection (P_I) by the corresponding probability of occurrence (P_P). In Figure **3** the probability density functions of individual infection risk (pdf_R), probability of infection (pdf_P), quanta concentration (pdf_n), and dose of quanta (pdf_D) after 2 hours of exposure are reported (in terms of R, P_I, n and D_q values for each percentile) for the illustrative example discussed above (i.e. scenario D, AER = 0.5 h^{-1}). The individual infection risk (R) presents a maximum value (R_{max}) at the 85th percentile (2.2%) due to a probability of infection P_I = 14.5% and a probability of occurrence P_P = 15%. In other words, the R value at the 85th percentile is the most probable individual infection risk for a healthy susceptible subject (i.e., the one with the highest chance of occurring). Due to the similarity of the probability density functions of the four expiration activities resulting from the calculation of the quanta emission rates ($\log_{10}(ER_q)$ reported in Table 2), the pdf_R for all the exposure scenarios tested here was similar to that of the exposure scenario shown in Figure 3 (i.e. the R_{max} value occurs in the narrow range of 84th–90th percentile).

Furthermore, as discussed in section 2.2, the probability density function of the probability of infection (pdf_P) is mostly influenced by the probability density function of the quanta emission rate (pdf_q) when moving backwards in the four-step approach; indeed, once the exposure scenario is defined, all the parameters contributing to the calculation of P_I (ventilation, room volume, subject

activity, etc.) can be considered as constant values. Thus, for a simplified estimate of R_{max}, the simplest calculation can be applied (instead of the Monte Carlo method) by just adopting the 85th percentile of the quanta emission rate in the four-step calculation using eqs. (2-4).

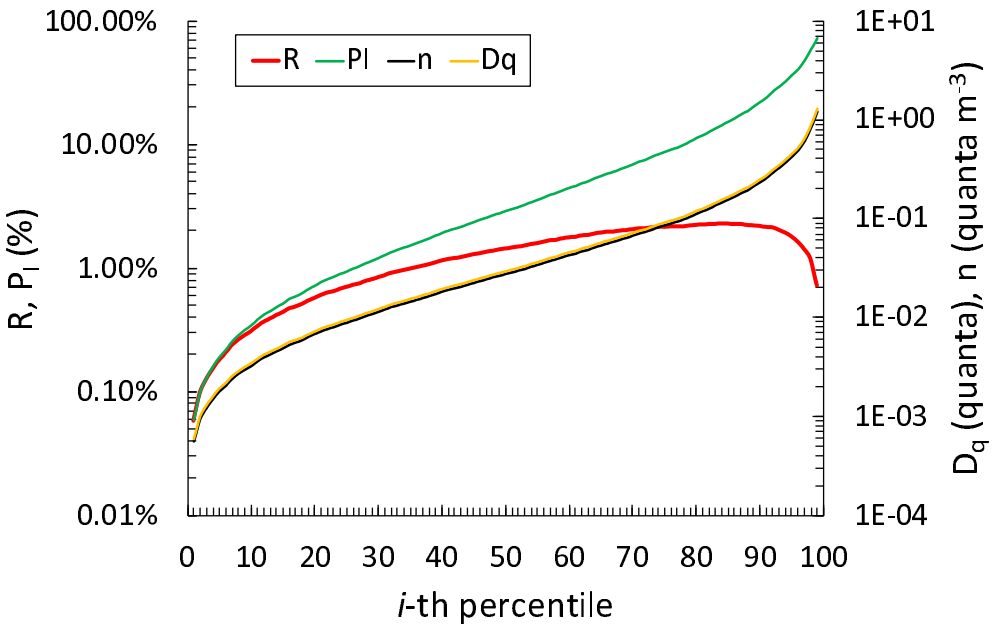

Figure 3 – Probability density functions of individual infection risk, probability of infection, quanta concentration, and dose of quanta at t = 120 min for the illustrative example reported in Figure **2** (exposure scenario A with an air exchange rate of 0.5 h^{-1}). The probability density functions are reported as quanta concentration (*n*), dose of quanta (D_q), probability of infection (P_I), and individual infection risk (R) for each percentile. The maximum individual infection risk (R_{max}) is 1.9% and occurs at the 85th percentile (P_I = 14.5%, P_q = 15%).

3.2.2 Estimate of the maximum individual risk versus exposure time in indoor environments

Figure 4 and Table 3 show the results of the Monte Carlo simulations for the four exposure scenarios analyzed. The exposure time–risk relationships reported in Figure 4 are essential as they can be used by choosing either the exposure time or the maximum risk R_{max} as the independent variable. In the first case, knowing the exposure time of the healthy subject in the environment in question, the corresponding individual infection risk can be evaluated and then compared to an

acceptable infection risk. In the second case, once an acceptable infection risk has been imposed, the corresponding maximum exposure time value can be easily assessed. The four scenarios are examined assuming an acceptable risk value of 10^{-3} as discussed in section 2.3. Since the maximum value of individual risk occurs roughly at the 90^{th} percentile, the corresponding probability of occurrence of the risk (P_P) is 10%; thus, an acceptable individual infection risk of 10^{-3} will roughly correspond to a probability of infection of P_I = 1%. For indoor environments characterized by high crowding indexes a P_I < 1% is essential as it can assure a R_0 < 1 when crowded with up to 100 people. Therefore, assuring an individual infection risk of 10^{-3} also guarantees the control of the epidemic with an R_0 < 1 for a maximum number of exposed healthy people S < 100.

For the exposure scenario discussed above (scenario D, AER = 0.5 h^{-1}) the maximum exposure time to reach an accepted risk of R = 10^{-3} is very short (16 min); this is due to the high viral load emitted during singing or speaking loudly leading to high quanta concentrations despite the large volume available. Obviously, the exposure time can increase with higher ventilation rates, e.g. reaching 38 min in the case of mechanical ventilation at 10 h^{-1}. The crowding index of such an indoor environment (800 m^3) ranges from 0.75 m^2 (auditorium) to 2 m^2 (conference room) per person [37]; thus, for a room height of 4 m a corresponding floor area of 200 m^2 will be available, then resulting in a total number of people simultaneously present in the room (S) ranging from 100 (conference room) to 267 (auditorium). Therefore, after 16 min of exposure in the case of natural ventilation (or 38 min in the case of mechanical ventilation with AER = 10 h^{-1}), the value of R_0 will be higher (auditorium) or equal (conference room) to 1. Thus, in the management of the epidemic, reducing the crowding index could be essential. Accepting higher R_{max} values would clearly increase the maximum exposure time; indeed, in the case of $R_{max} = 10^{-2}$, the exposure time values would be 62 min and 392 min, for an AER equal to 0.5 h^{-1} and 10 h^{-1}, respectively. However,

446 in this case, the corresponding value of R_0 would be lower than 1 only for a number of exposed
447 subjects lower than 10.
448 In scenario C, the infected subject in light activity speaks in a 300 m^3 environment, along with the
449 healthy subject. The simultaneous reduction of both the quanta emission rate and the volume
450 compared to scenario D makes the maximum exposure times for an acceptable infection risk of 10^{-3}
451 comparable to the previous case (15 min and 36 min for ventilation of 0.5 h^{-1} and 10 h^{-1},
452 respectively). Additionally, in this case, the estimated exposure times would guarantee an $R_0 < 1$
453 with $S < 100$ subjects.
454

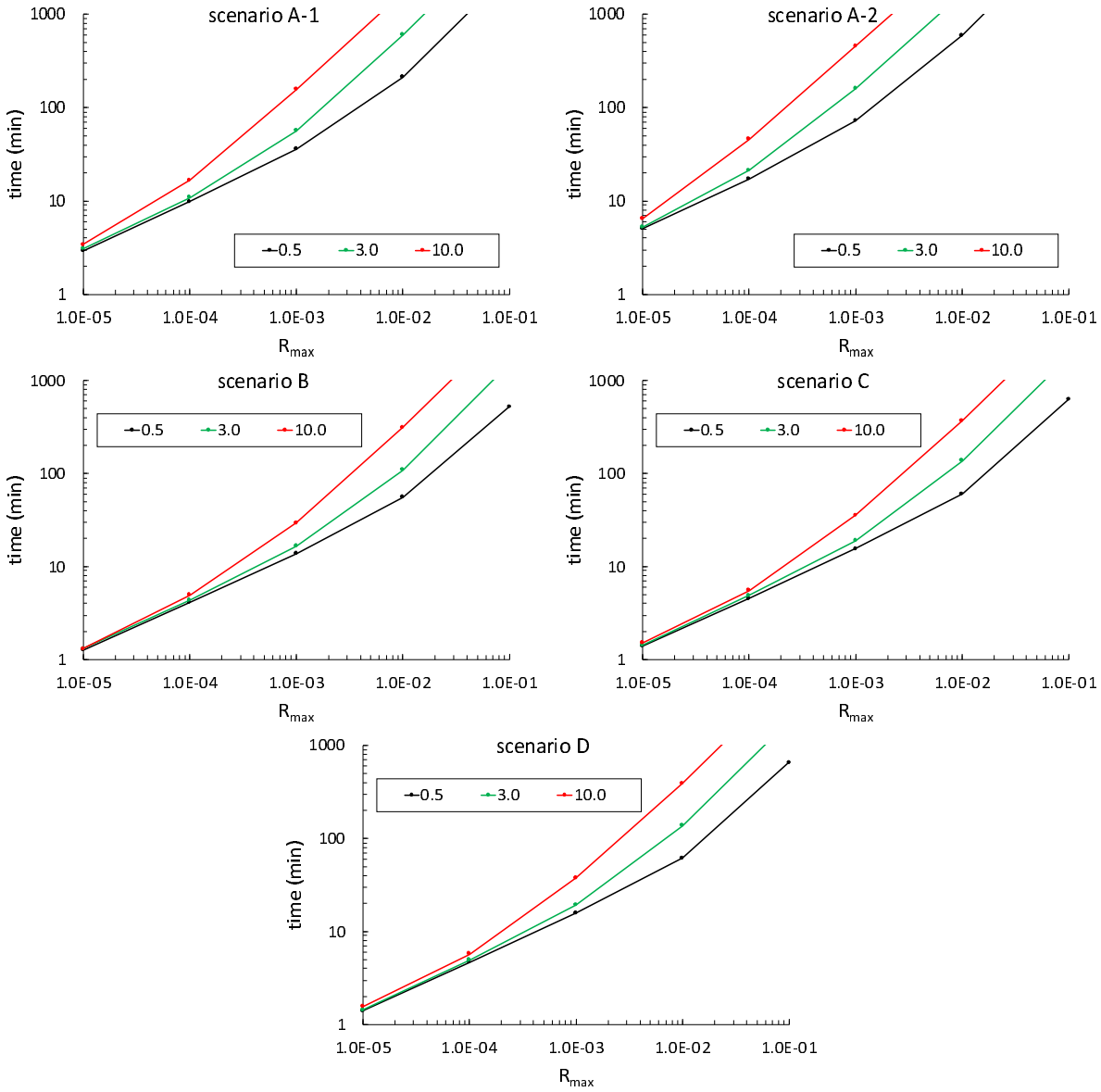

Figure 4 – Relationship between time of exposure and individual risk (R) as a function of the air exchange rate (0.5 h^{-1}, 3 h^{-1}, and 10 h^{-1}) for the exposure scenarios investigated in the prospective approach and summarized in Table 1.

In scenario A (patient emitting at rest in oral breathing), the maximum exposure time in a hospital room of 100 m^3 for both a medical staff member (scenario A-1) and a patient at rest without infection (scenario A-2) is evaluated. In both cases the exposure times increase significantly with the ventilation rate, reaching 36 min and 157 min (scenario A-1), and 72 min and 455 min (scenario A-2) with AER values of 0.5 h^{-1} and 10 h^{-1}, respectively. However, despite the small size

of the room, the ER_q was extremely small (Table 2); thus, unless a large number of infected subjects is simultaneously present in the room, the concentration of viral load in a hospital room can be considered low; nonetheless, the overall risk may become relevant due to the long exposure times (of 36 and 157 min). Finally, in exposure scenario B (the gym with infected and healthy subjects during heavy activity with oral breathing), although there is no vocalization in the subject's activity, the high inhalation rate produces considerable ER_q values, then increasing the individual risk; thus, in order to guarantee an acceptable infection risk of 10^{-3} the maximum exposure times resulted quite short, i.e. 14 min and 29 min for 0.5 h^{-1} and 10 h^{-1}, respectively. Thus, for all the scenarios investigated, the ventilation conditions strongly influence the risk (or the exposure time) of the exposed subject: this difference increases as the accepted risk increases as shown in the trends presented in Figure 4. In contrast, if a lower risk was accepted (i.e. 10^{-4} or 10^{-5}), increasing the air exchange rate is not leading to the significant reduction of the risk, and local exhaust ventilation would be more effective.

Table 3 – Maximum exposure time (min) for the different exposure scenarios to reach an acceptable maximum individual infection risk (R_{max}).

Exposure scenarios	AER (h^{-1})	**Maximum individual infection risk (R_{max})**				
		1×10^{-1}	1×10^{-2}	1×10^{-3}	1×10^{-4}	1×10^{-5}
Scenario A-1 - Hospital room	0.5	2797	212	36	10	3
Emitting subject: patient	3.0	7968	600	56	11	3
Exposed subject: Medical staff	10.0	22430	1727	157	17	3
Scenario A-2 - Hospital room	0.5	8039	597	72	17	5
Emitting subject: patient	3.0	21739	1678	159	21	5
Exposed subject: patient	10.0	64333	4671	455	46	6
Scenario B – Gym	0.5	519	55	14	4	1
Emitting subject: Exercising person	3.0	1500	110	16	4	1

Exposed subject: Exercising person	10.0	4119	314	29	5	1
Scenario C – Public indoors	0.5	627	60	15	5	1
Emitting subject: Speaking person	3.0	1812	137	19	5	1
Exposed subject: Speaking person	10.0	4807	372	36	6	1
Scenario D – Conference room	0.5	652	62	16	5	1
Emitting subject: Singer	3.0	1826	138	19	5	1
Exposed subject: Spectator	10.0	5187	392	38	6	2

3.3 Retrospective assessment application: the outbreaks in a restaurant in Guangzhou and at a choir rehearsal in Skagit Valley

Figure 5 shows the trends of quanta concentration and probability of infection (P_I) evaluated for the retrospective cases defined in section 2.4 (a restaurant in Guangzhou and the Skagit Valley choir). The retrospective analysis applied to the restaurant in Guangzhou (Figure 5a) revealed that, under the boundary conditions considered in the simulation (in terms of room volume, ventilation, number of exposed people; see section 2.4.1), a probability of infection (P_I) after 1 hour of exposure equal to the attack rate (45%) can be reached for a quanta emission rate of $ER_q = 61$ quanta h^{-1}. This emission rate, for an emitting subject speaking during light exercise, occurs at the 93rd percentile of the probability density function of ER_q (P_q).

Similarly, for the retrospective analysis applied to the Skagit Valley choir (Figure 5b), in order to reach an attack rate of 53% after 2.5 hours of exposure under the simulation boundary conditions reported in section 2.4.2, a quanta emission rate of 341 quanta h^{-1} is needed. Additionally, in this case, such an emission rate occurs at the 92nd percentile of the probability density function (P_q) of an infected subject while singing.

Therefore, for both the analyzed cases in the retrospective analyses, the required ER_q values to obtain the documented R_e fall perfectly within the possible values of the emission profiles under consideration (i.e. speaking and singing/speaking loudly in light activity reported in Table 2).

497 Moreover, such emission values incur high individual infection risks as they are around the 90th
498 percentile, i.e. at the percentile maximizing the individual infection risk (R_{max}). Indeed, the R values
499 for the restaurant at Guangzhou and the Skagit Valley choir were 3.2% and 3.7%, respectively –
500 more than one order of magnitude higher than the acceptable risk of 10^{-3}. In these two cases, an
501 individual risk of $< 10^{-3}$ would have been obtained with a probability of infection P_I = 1.3-1.4%:
502 such a P_I is not actually achievable by varying and optimizing the room ventilation (e.g.
503 AER > 100 h^{-1} would be required), and is achievable only by reducing the exposure time of the
504 susceptible subjects and the quanta emission rates.

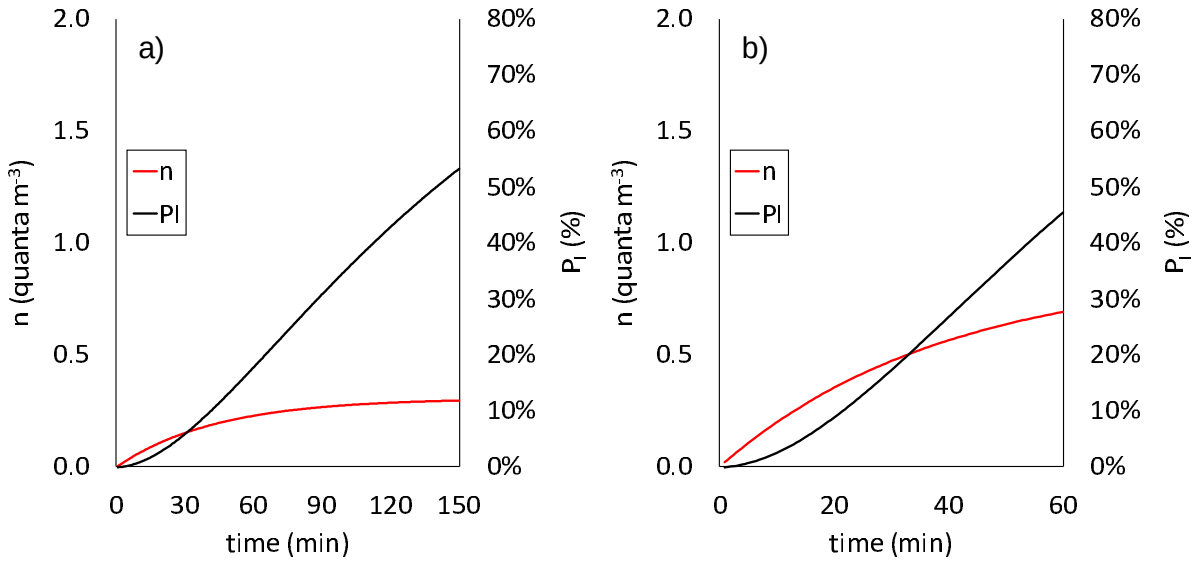

505

506 **Figure 5** – Quanta concentration (n) and probability of infection (P_I) evaluated for the retrospective cases
507 applied at the documented outbreaks at (a) the restaurant in Guangzhou and (b) the Skagit Valley choir.

508 To summarize, the retrospective assessment of the two SARS-CoV-2 outbreaks investigated
509 demonstrate that the documented number of infected people can be explained by means of the
510 airborne transmission route; indeed, the most probable of the expected events occurred. The
511 approach and consequent calculation reported here clearly highlights that the explanation of such
512 a high number of infected people does not necessarily require the presence of a superspreader in
513 the environment (i.e. an infected person with the highest viral load, c_v, and infectious dose, c_i), but

514 rather a co-existence of conditions, including emission and exposure parameters, leading to a

515 highly probable event, which can be defined as a “superspreading event”.

516

517

References

(1) Ai, Z. T.; Melikov, A. K. Airborne Spread of Expiratory Droplet Nuclei between the Occupants of Indoor Environments: A Review. *Indoor Air* **2018**, *28* (4), 500–524. https://doi.org/10.1111/ina.12465.

(2) Holmgren, H.; Ljungström, E.; Almstrand, A.-C.; Bake, B.; Olin, A.-C. Size Distribution of Exhaled Particles in the Range from 0.01 to 2.0µm. *Journal of Aerosol Science* **2010**, *41* (5), 439–446. https://doi.org/10.1016/j.jaerosci.2010.02.011.

(3) van Doremalen, N.; Bushmaker, T.; Morris, D. H.; Holbrook, M. G.; Gamble, A.; Williamson, B. N.; Tamin, A.; Harcourt, J. L.; Thornburg, N. J.; Gerber, S. I.; Lloyd-Smith, J. O.; de Wit, E.; Munster, V. J. Aerosol and Surface Stability of SARS-CoV-2 as Compared with SARS-CoV-1. *N Engl J Med* **2020**. https://doi.org/10.1056/NEJMc2004973.

(4) Ai, Z. T.; Hashimoto, K.; Melikov, A. K. Airborne Transmission between Room Occupants during Short-Term Events: Measurement and Evaluation. *Indoor Air* **2019**, *29* (4), 563–576. https://doi.org/10.1111/ina.12557.

(5) Ai, Z. T.; Huang, T.; Melikov, A. K. Airborne Transmission of Exhaled Droplet Nuclei between Occupants in a Room with Horizontal Air Distribution. *Building and Environment* **2019**, *163*, 106328. https://doi.org/10.1016/j.buildenv.2019.106328.

(6) Morawska, L.; Johnson, G. R.; Ristovski, Z. D.; Hargreaves, M.; Mengersen, K.; Corbett, S.; Chao, C. Y. H.; Li, Y.; Katoshevski, D. Size Distribution and Sites of Origin of Droplets Expelled from the Human Respiratory Tract during Expiratory Activities. *Journal of Aerosol Science* **2009**, *40* (3), 256–269. https://doi.org/10.1016/j.jaerosci.2008.11.002.

(7) Morawska, L.; Cao, J. Airborne Transmission of SARS-CoV-2: The World Should Face the Reality. *Environment International* **2020**, *139*, 105730. https://doi.org/10.1016/j.envint.2020.105730.

(8) Chao, C. Y. H.; Wan, M. P.; Morawska, L.; Johnson, G. R.; Ristovski, Z. D.; Hargreaves, M.; Mengersen, K.; Corbett, S.; Li, Y.; Xie, X.; Katoshevski, D. Characterization of Expiration Air Jets and Droplet Size

Distributions Immediately at the Mouth Opening. *Journal of Aerosol Science* **2009**, *40* (2), 122–133. https://doi.org/10.1016/j.jaerosci.2008.10.003.

(9) Morawska, L. Droplet Fate in Indoor Environments, or Can We Prevent the Spread of Infection? *Indoor Air* **2006**, *16* (5), 335–347. https://doi.org/10.1111/j.1600-0668.2006.00432.x.

(10) Hickey, A. J.; Mansour, H. M. *Inhalation Aerosols: Physical and Biological Basis for Therapy, Third Edition*; Taylor & Francis Ltd, 2019.

(11) Duguid, J. P. The Numbers and the Sites of Origin of the Droplets Expelled during Expiratory Activities. *Edinburgh Medical Journal* **1945**, *LII (II)* (II), 385–401.

(12) Jennison, M. W. Atomizing of Mouth and Nose Secretions into the Air as Revealed by High Speed Photography. *Aerobiology* **1942**, *17*, 106–128.

(13) Wells, W. F. On Airborne Infection: Study II. Droplets and Droplet Nuclei. *American Journal of Epidemiology* **1934**, *20* (3), 611–618. https://doi.org/10.1093/oxfordjournals.aje.a118097.

(14) Tang, J. W.; Noakes, C. J.; Nielsen, P. V.; Eames, I.; Nicolle, A.; Li, Y.; Settles, G. S. Observing and Quantifying Airflows in the Infection Control of Aerosol- and Airborne-Transmitted Diseases: An Overview of Approaches. *Journal of Hospital Infection* **2011**, *77* (3), 213–222. https://doi.org/10.1016/j.jhin.2010.09.037.

(15) Myatt, T. A.; Minegishi, T.; Allen, J. G.; Macintosh, D. L. Control of Asthma Triggers in Indoor Air with Air Cleaners: A Modeling Analysis. *Environ Health* **2008**, *7*, 43. https://doi.org/10.1186/1476-069X-7-43.

(16) Rudnick, S. N.; Milton, D. K. Risk of Indoor Airborne Infection Transmission Estimated from Carbon Dioxide Concentration. *Indoor Air* **2003**, *13* (3), 237–245. https://doi.org/10.1034/j.1600-0668.2003.00189.x.

(17) Sze To, G. N.; Chao, C. Y. H. Review and Comparison between the Wells–Riley and Dose-Response Approaches to Risk Assessment of Infectious Respiratory Diseases. *Indoor Air* **2010**, *20* (1), 2–16. https://doi.org/10.1111/j.1600-0668.2009.00621.x.

(18) Wagner, B. G.; Coburn, B. J.; Blower, S. Calculating the Potential for Within-Flight Transmission of Influenza A (H1N1). *BMC Medicine* **2009**, *7* (1), 81. https://doi.org/10.1186/1741-7015-7-81.

(19) Buonanno, G.; Stabile, L.; Morawska, L. Estimation of Airborne Viral Emission: Quanta Emission Rate of SARS-CoV-2 for Infection Risk Assessment. *Environment International* **2020**. https://doi.org/10.1101/2020.04.12.20062828.

(20) Gammaitoni, L.; Nucci, M. C. Using a Mathematical Model to Evaluate the Efficacy of TB Control Measures. *Emerging Infectious Diseases* **1997**, 335–342.

(21) Riley, C.; Murphy, G.; Riley, R. L. Airborne Spread of Measles in a Suburban Elementary School. *American journal of epidemiology* **1978**, No. 107, 431–432.

(22) Hammersley, J. M.; Handscomb, D. C. *Monte Carlo Methods*; Chapman and Hall: London & New York, 1964.

(23) Pan, Y.; Zang, D.; Yang, P.; Poon, L. M.; Wang, Q. Viral Load of SARS-CoV-2 in Clinical Samples Yang Pan Daitao Zhang Peng Yang Leo L M Poon Quanyi Wang. *The Lancet* **2020**.

(24) Rothe, C.; Schunk, M.; Sothmann, P.; Bretzel, G.; Froeschl, G.; Wallrauch, C.; Zimmer, T.; Thiel, V.; Janke, C.; Guggemos, W.; Seilmaier, M.; Drosten, C.; Vollmar, P.; Zwirglmaier, K.; Zange, S.; Wölfel, R.; Hoelscher, M. Transmission of 2019-NCoV Infection from an Asymptomatic Contact in Germany. *N Engl J Med* **2020**, *382* (10), 970–971. https://doi.org/10.1056/NEJMc2001468.

(25) To, K. K.-W.; Tsang, O. T.-Y.; Leung, W.-S.; Tam, A. R.; Wu, T.-C.; Lung, D. C.; Yip, C. C.-Y.; Cai, J.-P.; Chan, J. M.-C.; Chik, T. S.-H.; Lau, D. P.-L.; Choi, C. Y.-C.; Chen, L.-L.; Chan, W.-M.; Chan, K.-H.; Ip, J. D.; Ng, A. C.-K.; Poon, R. W.-S.; Luo, C.-T.; Cheng, V. C.-C.; Chan, J. F.-W.; Hung, I. F.-N.; Chen, Z.; Chen, H.; Yuen, K.-Y. Temporal Profiles of Viral Load in Posterior Oropharyngeal Saliva Samples and Serum Antibody Responses during Infection by SARS-CoV-2: An Observational Cohort Study. *The Lancet Infectious Diseases* **2020**. https://doi.org/10.1016/S1473-3099(20)30196-1.

(26) Woelfel, R.; Corman, V. M.; Guggemos, W.; Seilmaier, M.; Zange, S.; Mueller, M. A.; Niemeyer, D.; Vollmar, P.; Rothe, C.; Hoelscher, M.; Bleicker, T.; Bruenink, S.; Schneider, J.; Ehmann, R.; Zwirglmaier, K.; Drosten, C.; Wendtner, C. Clinical Presentation and Virological Assessment of Hospitalized Cases of Coronavirus Disease 2019 in a Travel-Associated Transmission Cluster. *medRxiv* **2020**, 2020.03.05.20030502. https://doi.org/10.1101/2020.03.05.20030502.

(27) Watanabe, T.; Bartrand, T. A.; Weir, M. H.; Omura, T.; Haas, C. N. Development of a Dose-Response Model for SARS Coronavirus. *Risk Anal* **2010**, *30* (7), 1129–1138. https://doi.org/10.1111/j.1539-6924.2010.01427.x.

(28) Yang, W.; Marr, L. C. Dynamics of Airborne Influenza A Viruses Indoors and Dependence on Humidity. *PLOS ONE* **2011**, *6* (6), e21481. https://doi.org/10.1371/journal.pone.0021481.

(29) Chatoutsidou, S. E.; Lazaridis, M. Assessment of the Impact of Particulate Dry Deposition on Soiling of Indoor Cultural Heritage Objects Found in Churches and Museums/Libraries. *Journal of Cultural Heritage* **2019**, *39*, 221–228. https://doi.org/10.1016/j.culher.2019.02.017.

(30) Haas, C. N. Estimation of Risk Due to Low Doses of Microorganisms: A Comparison of Alternative Methodologies. *Am J Epidemiol* **1983**, *118* (4), 573–582. https://doi.org/10.1093/oxfordjournals.aje.a113662.

(31) Cotruvo, J. A. Drinking Water Standards and Risk Assessment. *Regul Toxicol Pharmacol* **1988**, *8* (3), 288–299. https://doi.org/10.1016/0273-2300(88)90016-5.

(32) World Health Organization. *Guidelines for Drinking-Water Quality - 4th Edition*; WHO Regional Office for Europe, 2011.

(33) Toner, G. *Innovation, Science, Environment 08/09*; McGill-Queen's University Press, 2008.

(34) Lu, J.; Gu, J.; Li, K.; Xu, C.; Su, W.; Lai, Z.; Zhou, D.; Yu, C.; Xu, B.; Yang, Z. COVID-19 Outbreak Associated with Air Conditioning in Restaurant, Guangzhou, China, 2020. *Emerg Infect Dis* **2020**, *26* (7). https://doi.org/10.3201/eid2607.200764.

(35) Hamner, L.; Dubbel, P.; Capron, I.; Ross, A.; Jordan, A.; Lee, J.; Lynn, J.; Ball, A.; Narwal, S.; Russell, S.; Patrick, D.; Leibrand, H. High SARS-CoV-2 Attack Rate Following Exposure at a Choir Practice - Skagit County, Washington, March 2020. *Morbidity and Mortality Weekly Report* **2020**, *69*.

(36) Asadi, S.; Wexler, A. S.; Cappa, C. D.; Barreda, S.; Bouvier, N. M.; Ristenpart, W. D. Aerosol Emission and Superemission during Human Speech Increase with Voice Loudness. *Scientific Reports* **2019**, *9* (1), 2348. https://doi.org/10.1038/s41598-019-38808-z.

(37) European Committee for Standardisation. UNI EN 15251 - Indoor Environmental Input Parameters for Design and Assessment of Energy Performance of Buildings Addressing Indoor Air Quality, Thermal Environment, Lighting and Acoustics. **2008**.